

Joint torque sensing for the upper-body of the iCub humanoid robot

Alberto Parmiggiani, Marco Randazzo, Lorenzo Natale, Giorgio Metta, Giulio Sandini

Department of Robotics, Brain and Cognitive Sciences

Italian Institute of Technology

Via Morego 30, Genova, ITALY

{alberto.parmiggiani,marco.randazzo,lorenzo.natale,giorgio.metta,giulio.sandini}@iit.it

Abstract—This paper describes the design and integration of three joint torque sensors on the arm of the iCub platform [1], [2]. The objective is to enhance the robot arm with joint torque control capability. This activity is part of a general upgrade of the humanoid robot to provide the entire 53 degree of freedom robot with low-level joint torque control. In particular, the shoulder is challenging because of the complex and compact mechanism of the shoulder. We first modeled the behaviour of the sensors with analytical equations and the sensor geometry were subsequently optimized using finite element structural simulations. The sensors were then constructed, and integrated in the arm assembly. Finally we present preliminary experiments to validate the design.

I. INTRODUCTION

One of the current trends in robotics is to develop applications for everyday life: the “natural” robot domain is thus gradually shifting from highly structured factory workshops to human environments [3]. As this happens interactions with humans and the environment will become not only unavoidable but also necessary. In this scenario we can easily foresee the occurrence of unmodeled and unexpected impacts. Traditionally the robots’ actuation relies on the use of electric motors coupled with high ratio speed reducers. This causes a high mechanical impedance which in turn makes the robots very stiff and poses several issues in terms of safety.

Bicchi et al. and Zinn et al. first introduced the problematics related to robotics safety in [4] and [5] respectively whereas more recently the safety of light-weight robots has been systematically tested [6], [7].

A general solution to the problem is to increase the robots’ compliance. Compliance can be introduced passively by elastically decoupling the actuation and the driven link (see [8] for a review). An alternative is to implement compliance actively relying on fast force and torque feedback loops. Although this approach has some disadvantages (lack of intrinsic safety, not energy efficient) it doubtlessly has the advantage of reducing the additional mechanical complexity of the final implementation.

To do this the standard method in the industrial automation field is to equip robotic manipulators with force-torque sensors located near the end effector, implicitly assuming that all interactions with the environment will occur in this part of the robot. However this solution proves to be only partially satisfactory for robots interacting in complex unstructured

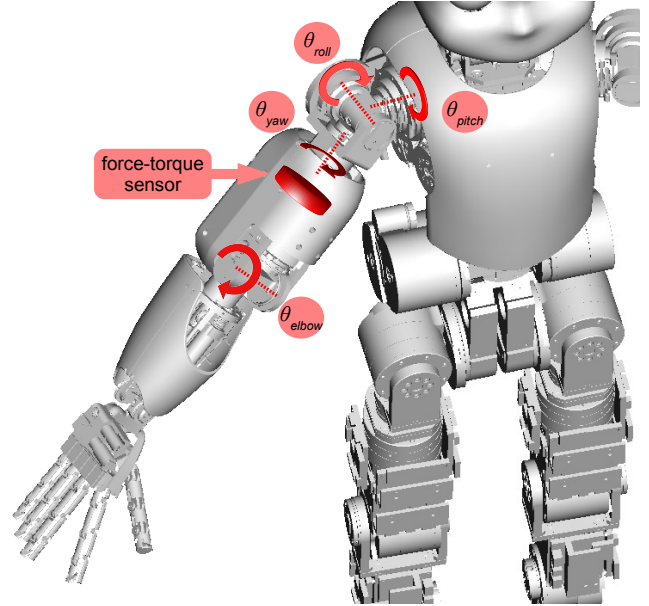


Fig. 1. The iCub arm. A CAD view of the arm of the iCub robot with superimposed joint labels (θ_{pitch} for shoulder pitch, θ_{roll} for shoulder roll, θ_{yaw} for shoulder roll and θ_{elbow} for the elbow rotation). The figure also represents the approximate position of the six axis force torque sensor integrated in the arm

environments. The implementation of suitable controllers (as in [9], [10]) requires the measurement of torques at joint level.

We therefore decided to enhance the iCub open platform [1] with joint torque sensing capability. In this paper we address the design of joint torque sensors and their integration on the upper-body of the iCub robot.

Before undertaking the single joint sensorization we considered exploiting the informations provided by the six-axis force-torque sensor located in the upper arm structure. To do this one would need to decouple the sensed force and torque components and project to the joint space. Besides requiring a kinematic model of the arm this decoupling is position dependent because it varies with the arm configuration.

The decoupling would have to be performed on the DSPs controlling the motors [11] at the cost of introducing latencies in the controller and increasing the overall computational load. Moreover this solution would not allow to measure interactions

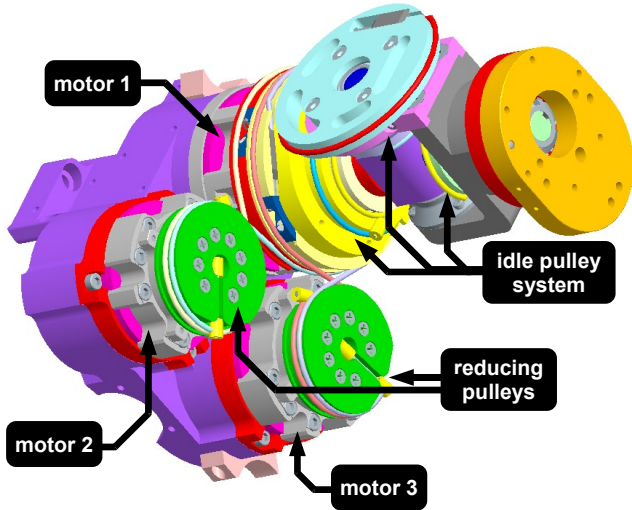


Fig. 2. The shoulder joint. A CAD view of the shoudler joint mechanism indicating the three motors actuating the joint and the pulley system.

occurring between the sensor and the torso of the robot.

II. ICUB ARM STRUCTURE

The scope of the current work was limited to the main joints of the arms of the iCub, neglecting for the moment the forearm and wrist joints, which are less critical for our purposes

The arm joints constitute a 4DoF manipulator with one rotational 3DoF proximal “shoulder” joint and a rotational distal “elbow” joint (see Fig.I).

The arm also comprises a six-axis force-torque sensor [11] located immediately after the shoulder joint.

The shoulder joint is based on a cable differential mechanism similar to the one introduced by Salisbury et. al. in [12] which basically constitutes a coupled transmission system (see Fig.II). It transforms the power output of three motors housed in the upper-torso, into the spherical motion of the shoulder.

The motor groups are based on the combination of a harmonic drive reduction (CSD series with 100:1 ratio) and a brushless frameless motor (RBE Kollmorgen series). The “torso” aluminum frame houses three of such motor groups: one high power actuator group (labelled “motor 1” in Fig.II) capable of delivering 40Nm and two medium power motor groups (“motor 2” and “motor 3”) providing 20Nm each.

The first motor actuates directly the first joint whereas the second and third motors actuate two pulleys that are coaxial with the first motor. These pulleys have slightly different primitive diameters thus producing a transmission reduction r^{-1} equal to the ratio of their diameters:

$$r = 40mm/65mm \approx 0.615385 \quad 1/r = 1.625 \quad (\text{II.1})$$

¹We adopted the following conventions for our notation: scalars are denoted by lower case letters in italic face (e.g., r), vectors are denoted by lower case letters in bold face (e.g., θ), matrices are denoted by upper case letters in bold face (e.g., T), $^{-1}$ denotes the inverse of a matrix, and t denotes the transpose of a vector or matrix. All vectors are originally column vectors. Dots on top of variables indicate time derivatives.

The pulley motion is then transmitted to the shoulder roll and pitch joints through a set of idle pulleys.

This whole mechanism results in a coupled 3DoF joint where the coupling between the angular velocities at the motors $[\dot{\theta}_{m1}, \dot{\theta}_{m2}, \dot{\theta}_{m3}]^t = \dot{\theta}_m$ and at the joints $[\dot{\theta}_{pitch}, \dot{\theta}_{roll}, \dot{\theta}_{yaw}]^t = \dot{\theta}_j$ is mapped by the following linear transformation matrix T :

$$\dot{\theta}_m = T\dot{\theta}_j \quad T = \begin{bmatrix} 1 & 0 & 0 \\ -r & r & 0 \\ -2r & r & r \end{bmatrix} \quad (\text{II.2})$$

by writing the power p conservation equation:

$$p = \tau_j^t \dot{\theta}_j = \tau_m^t \dot{\theta}_m \quad (\text{II.3})$$

$$\begin{aligned} \tau_j^t \dot{\theta}_j &= \tau_m^t T \dot{\theta}_j \\ \tau_j^t \dot{\theta}_j &= (T^t \tau_m)^t \dot{\theta}_j \quad \forall \dot{\theta}_j \\ \tau_j &= T^t \tau_m \end{aligned}$$

$$\tau_m = T^{-t} \tau_j \quad (\text{II.4})$$

we obtain that the torques at joint level can be transformed to the torques at motor level through the inverse transposed of matrix T :

$$T^{-t} = \begin{bmatrix} 1 & -1 & 1 \\ 0 & 1/r & -1/r \\ 0 & 0 & 1/r \end{bmatrix} \quad (\text{II.5})$$

This special joint design allows for optimizations of the robot mass distribution resulting in an extremely compact and light-weight manipulator. The iCub arm thus exhibits a payload-to-weight ratio of 0.45 which is comparable to those achieved by other state-of-the-art robots with joint level torque control (0.25 for the Barrett WAM [13] and 1.0 for the DLR LWR III [10]), although its design is favoured by the relatively short link lengths. However this particular manipulator design is more difficult to control: to obtain the motion of a single joint it is necessary to actuate all the three shoulder motors.

Other complexities arise when trying to close a feedback loop: to track the errors measured at joint level these need to be transformed at motor level with additional computation to be performed by the DSPs controlling the motors.

An additional problem is constituted by the joint position sensing. Because of space limitations it was unfeasible to integrate an encoder directly on the yaw axis. The missing information was recovered by placing the encoder on the axis of motor 3. The observed positions $\theta_o = [\theta_{pitch}, \theta_{roll}, \theta_{m3}]^t$ are then mapped to the actual joint positions θ_j with the following transformation matrix:

$$\theta_j = R\theta_o \quad R = \begin{bmatrix} 1 & 0 & 0 \\ 0 & 1 & 0 \\ 1 & -1 & 1/r \end{bmatrix} \quad (\text{II.6})$$

III. JOINT TORQUE SENSORS DESIGN

By referring to studies found in the literature such as those by Aghili et al. [14], Hirzinger et al. [9] and Visser et al. [15] we started this project with the following set of specifications:

- 1) high frequency and resolution joint level torque feedback: as described in [10], [16] a high frequency torque feedback loop is essential for smooth control; we considered a 1kHz rate to be sufficient for our application. For what concerned the resolution we aimed for 16bits over a dynamic range of 40Nm for all the joints.
- 2) full electronic and mechanical retro-compatibility: the hardware upgrade had to be considered as a sort of “plug-in” and was thus required to seamlessly integrate on the current robot structure.

The second requirement was particularly difficult to fulfill because it implied that the upgrade should not have interfered with any of the functional part dimensions, therefore restricting significantly our possibilities at the design stage.

A. Semi-conductor strain gauges

Torque is generally measured indirectly by measuring the deformation of a part through which torque is transmitted: if linear elasticity conditions hold, torque is directly proportional to the measured deformation. To increase the signal to noise ratio and to obtain high resolution it is desirable to design a structure which can generate the highest possible strain. However this generally results in increasing the internal stresses in the part. The sensor design problem is thus complicated by two conflicting requirements: mechanical robustness and torque sensitivity.

To measure deformations metal-alloy strain gauges are widely employed: an alternative is constituted by semiconductor strain gauges (SSGs). In SSGs the change in resistivity depends on piezo-resistive effects of boron doped silicon. The semiconductor bonded strain gauge is a thin slice of silicon substrate with the resistance element diffused into a substrate of silicon. The wafer element usually is not provided with a backing, and bonding it to the strained surface requires great care as only a thin layer of epoxy is used to attach it. Although more expensive, SSGs have several advantages over standard metal strain gauges among which higher sensitivity (less deformation is needed to produce the same effect), higher fatigue life, higher output signal.

Since our application required a very high sensitivity and large signal to noise ratio SSGs were preferred over standard metal strain gauges. A drawback of SSGs is their attachment process, which is very delicate and requires long curing and settling times.

Moreover SSGs are very sensitive to temperature changes: the resistivity of these components drifts up to 10% for a 10°C temperature shift. The standard solution to cope with these temperature-caused resistivity drifts is to arrange four SSGs in a Wheatstone bridge configuration, or two in a half-bridge configuration: provided that the resistivity changes occurring in the different SSGs are similar the bridge remains balanced.

We conducted extensive tests on this issue and quantified the temperature induced voltage bias in 2% of the full scale value.

SSGs maintain a linear strain-resistivity behavior up to $\pm 1000\mu\epsilon$ while the maximum strain they can tolerate is $\pm 5000\mu\epsilon$. Their choice implied therefore an additional design constraint regarding the strain levels in the region of the deformable part where they were to be glued.

B. Conceptual design

We then faced the issue of integrating the torque sensing elements into our joints. To do this there are generally two alternatives: a first option is to redesign and sensorize one of the elements of the transmission chain whereas a second alternative is to insert in the transmission chain an additional controlled deformation transducer. This latter choice is generally easier to implement because it frees the designer of the dimensional constraints posed by the existing parts. Another important decision is whether to place the torque sensors at the joint level or at the motor level in the coupled shoulder joint (described in Sec.II). We decided to place the sensors at the joint level for two reasons: firstly we considered that it is most important to know the torques exerted by the robot rather than to simplify its controller; secondly placing the sensors at the motor level requires dimensional changes incompatible with the second design specification. Moreover introducing the sensors at joint level allows to compensate transmission nonlinearities (friction, elasticity) although makes the controller more complicated.

We then identified possible locations for the sensors in the current structure of the arm. Once we identified a plausible sensor placement the initial sensor geometry and dimensions were determined with the equations of linear elasticity [17]. The tentative sensor design was firstly validated with structural finite element analyses (FEAs) performed with the Ansys commercial software package. These analyses were then iterated several times to optimize critical geometric features.

The complex mechanism of the shoulder joint made the integration of the sensor for the pitch axis a rather difficult design problem. It was in the end decided to position the sensor directly on the motor output shaft. We firstly locally reduced the shaft cross-section to obtain strain levels tailored to the SSGs operating range. This particular placement however required to route the sensor wires out of the mechanism to the signal conditioning electronics. This issue was solved by designing a new hollow motor shaft that allowed to extract the cable from the rear of the motor (Fig.3). Because of the small spaces available and of the strong motor EMI we had to employ a special four-wire shielded micro-cable with 1.01mm outer diameter.

The sensor for the roll axis was made by adding a new part fixed to the transmission pulleys (Fig.4). The new part has two beam-like structures in its terminal part whose flexion is proportional to the transmitted torque.

For the shoulder yaw joint no new sensor was required since it coincides with the torque measured on the z axis by the six-axis force-torque sensor mounted after the shoulder joint.

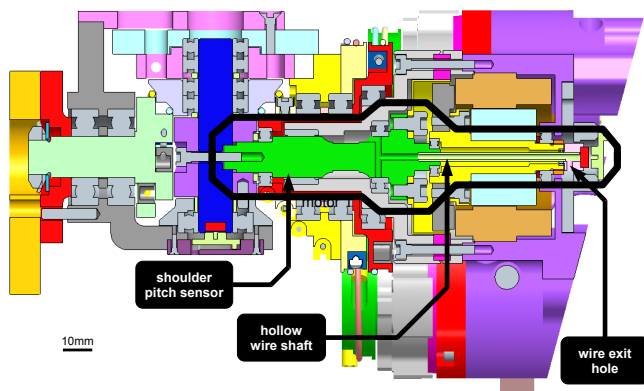


Fig. 3. Shoulder pitch sensor. The figure shows a CAD cross section of the new shoulder joint: the sensor and the wire shaft are labeled.

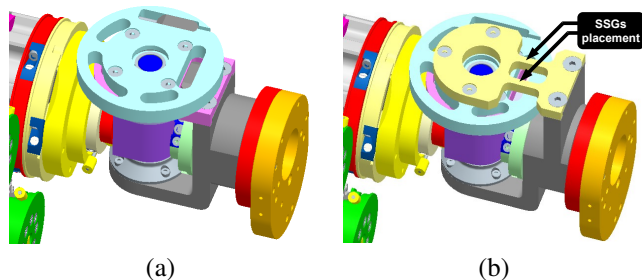


Fig. 4. Shoulder roll joint. The figure allows the comparison of the previous joint design (a) and its upgraded version (b).

The elbow joint was modified to insert a spoke-like structure: measuring the flexion of this part allowed to measure the torque exerted by the elbow joint (see Fig.5): this required however some minor changes of the bearings and their supports.

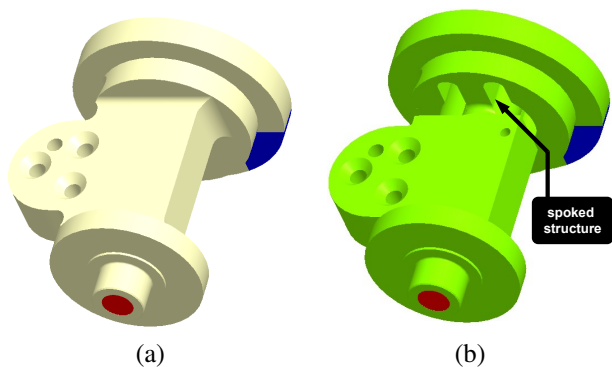


Fig. 5. Elbow joint upgrade. The figure shows the changes undergone by the elbow joint: the old version is shown in (a) whereas the new part is shown in (b).

C. Finite element analyses

We validated the design of the sensors with the help of FEAs. We processed the CAD models with the Ansys Educational FEA software. Since the sensors are not affected by relevant non-linearities we chose to perform a linear elastic analysis.

We chose to employ 36CrNiMo4 stainless steel for the shoulder pitch and elbow sensors to achieve high mechanical robustness. This material has a Young's modulus of 72000MPa, a Poissons' ratio of 0.33, and yields at about 1050MPa.

On the other hand the material we chose for the shoulder roll joint is an aluminum-zinc-magnesium-copper alloy named Ergal7075. This material has a lower Young's modulus so less force is required to induce measurable strains thus increasing the sensitivity of the sensor; its rather high mechanical resistance (520MPa ca. tensile strength) is also adequate for our design purposes. Its Young's modulus and Poissons' ratio are 72000MPa and 0.33 respectively.

The meshes for the FEAs were generated automatically with a patch independent tetrahedron algorithm with refinement conditions in the critical regions to better model the stress/strain gradients.

For what concerns the boundary conditions all the simulations were performed with a 40Nm torque. The screws used to fix the parts were modeled with a zero displacement (x , y , and z directions) condition. In the shoulder pitch and elbow sensors bearings were modeled by constraining the radial displacements of the surfaces they were acting on. In the shoulder roll joint to simulate simply the contact with the subjacent part the vertical displacements of the base of the sensor were constrained to be zero.

The results of the simulations are shown in Fig.6. The last iteration of the FEAs allowed to obtain in the region to be sensorized strain levels appropriate to the SSGs operating range ($\pm 500\mu\epsilon$ to $\pm 1000\mu\epsilon$).

IV. ELECTRONICS

We attached the three half-bridges to a six-channel signal conditioning board already used on the iCub six-axis force-torque sensor. The analog channels are firstly filtered (first-order RC), multiplexed, and amplified. The gain of the amplifier was chosen to measure finely joint torques in the range of $\pm 1.75\text{Nm}$ approximately. This gain is not suitable to cover the full range of the sensor (as it would cause a saturation of the amplifier) but it allows better to measure small torque variations.

The six channels are subsequently digitalized by a 16-bit ADC. It is furthermore possible to add to the digital datum a compensation offset value. These values were determined in the calibration phase. The calibration constant was calculated as the ratio between the digital data and the corresponding joint torque (computed from the links mass distribution derived from CAD).

A micro-controller filters the raw data (IIR low-pass at 80Hz) and performs some additional basic data pre-processing. The data are finally broadcast through a CAN bus interface at a frequency of 1kHz.

V. EXPERIMENTAL VALIDATION

Fig.7 shows the complete assembly of the sensorized arm. To test the effectiveness of our sensor we measured the

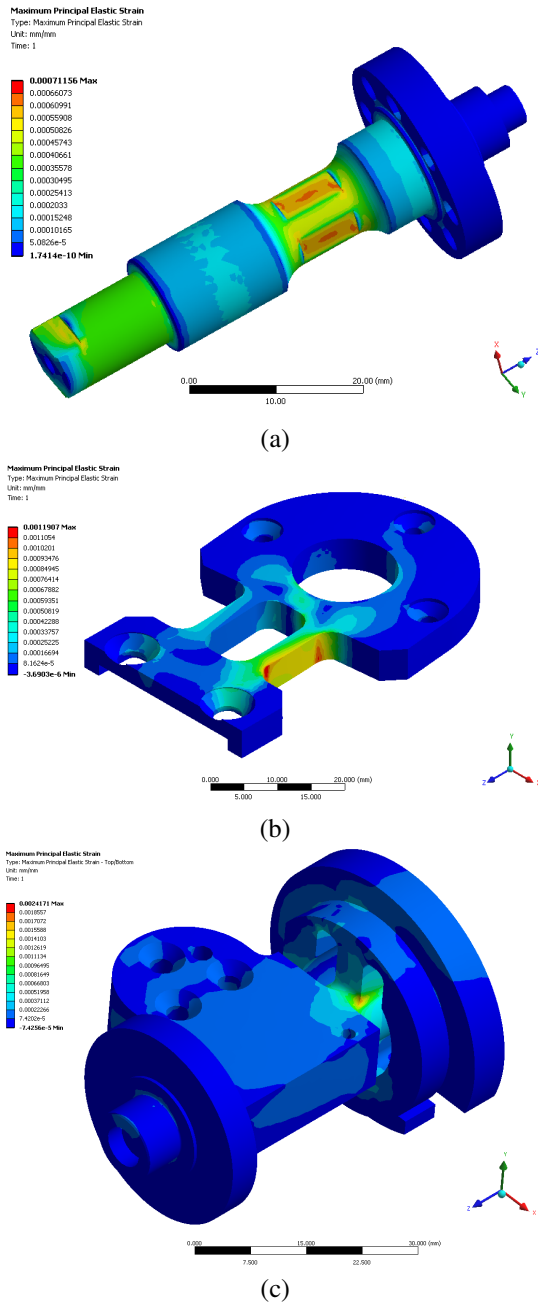


Fig. 6. Finite element analyses. The figure represents the simulated strain field for the shoulder pitch (a), shoulder roll (b), and elbow (c) joint sensors respectively.

gravitational torques at the joints and compared them with their expected value. The results of this test are shown in Fig.8. To trace the curves we measured static joint torques at various joint positions spanning from the joint range at 5deg increments. Some mismatches can be appreciated, specially for the elbow joint. Various reasons for these behaviours can be conjectured such as unmodeled frictional stiction effects or non-linear elastic characteristics in the steel tendons and the Harmonic-Drive reducers: further analyses in this sense are required. Moreover the shoulder yaw joint yields slightly more

noisy measures. The digital signals are in general affected by 2 to 3 bits of noise thus reducing the final resolution to 13 bits. Nevertheless sensor readings generally correlate nicely with the corresponding expected results.

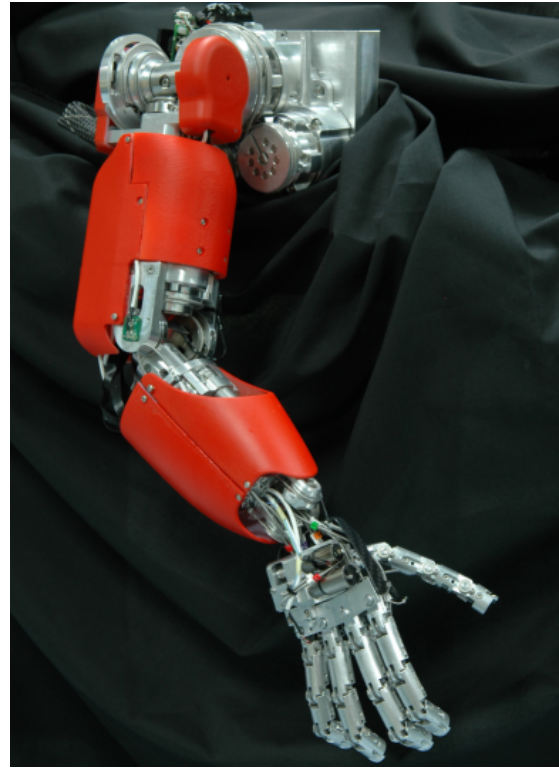


Fig. 7. iCub arm. The figure shows the final arm assembly integrating the joint torque sensors.

VI. CONCLUSIONS

In this paper we described the design process of joint torque sensors for the arm of the iCub open platform. We also discussed various aspects regarding their integration on the robot. We finally showed experimental data proving that our design is effective. This work is therefore intended as the basis for joint torque control of the main joints of the upper-body of the iCub humanoid robot.

ACKNOWLEDGMENTS

This work has been supported by the European Commission FP6 Project RobotCub IST-004370 and FP7 project CHRIS IST-215805.

We would like to thank and to acknowledge the contributions to this project of Claudio Lorini, Marco Maggiali, Bruno Bonino, the people working in the IIT Electronics Design Lab., Davide Gandini and Emiliano Barbieri, Roberto Puddu, Charlie Sanguineti and Mattia Salvi whose help has been essential to the completion of this work.

We would also like to thank Francesco Becchi for his assistance in the conceptual design of the shoulder pitch and elbow sensors.

REFERENCES

- [1] G. Metta, D. Vernon, L. Natale, F. Nori, and G. Sandini, "The icub humanoid robot: an open platform for research in embodied cognition," in *Performance Metrics for Intelligent Systems (PerMIS), 2008 Workshop on*, vol. NIST Special Publication 1090, August 2008, pp. 50–56.
- [2] "RobotCub website," <http://www.robotcub.org>, Jun. 2009.
- [3] A. De Santis, B. Siciliano, A. De Luca, and A. Bicchi, "An atlas of physical human-robot interaction," *Mechanism and Machine Theory*, vol. 43, no. 3, pp. 253–270, March 2008. [Online]. Available: <http://dx.doi.org/10.1016/j.mechmachtheory.2007.03.003>
- [4] A. Bicchi and G. Tonietti, "Fast and "soft-arm" tactics [robot arm design]," *Robotics & Automation Magazine, IEEE*, vol. 11, no. 2, pp. 22–33, June 2004. [Online]. Available: <http://dx.doi.org/10.1109/MRA.2004.1310939>
- [5] M. Zinn, O. Khatib, B. Roth, and J. K. Salisbury, "Playing it safe [human-friendly robots]," *Robotics & Automation Magazine, IEEE*, vol. 11, no. 2, pp. 12–21, 2004. [Online]. Available: <http://dx.doi.org/10.1109/MRA.2004.1310938>
- [6] S. Haddadin, A. A. Schaffer, and G. Hirzinger, "Safety evaluation of physical human-robot interaction via crash-testing," *Robotics: Science and Systems Conference (RSS 2007)*, 2007. [Online]. Available: <http://www.roboticsproceedings.org/rss03/p28.pdf>
- [7] S. Haddadin, A. Albu-Schaffer, M. Frommberger, and G. Hirzinger, "The role of the robot mass and velocity in physical human-robot interaction - part II: constrained blunt impacts," in *Robotics and Automation, 2008. Proceedings. ICRA '08. IEEE International Conference on*, vol. 2, 2008, pp. 1331–1338. [Online]. Available: <http://dx.doi.org/10.1109/ROBOT.2008.4543388>
- [8] R. Van Ham, T. Sugar, B. Vanderborght, K. Hollander, and D. Lefeber, "Review of actuators with passive adjustable compliance / controllable stiffness for robotic applications," *Robotics & Automation Magazine, IEEE*, vol. accepted for publication, 2009.
- [9] G. Hirzinger, J. Butterfass, M. H. M. Fischer M. Grebenstein, H. Liu, I. Schaefer, and N. Sporer, "A mechatronics approach to the design of light-weight arms and multifingered hands," in *Proc. IEEE Int. Conf on Robotics and Automation*, 2000, pp. 46–54.
- [10] G. Hirzinger, N. Sporer, A. Albu-Schaffer, M. Hahnle, R. Krenn, A. Pascucci, and M. Schedl, "DLR's torque-controlled light weight robot III-are we reaching the technological limits now?" in *Robotics and Automation, 2002. Proceedings. ICRA '02. IEEE International Conference on*, vol. 2, 2002, pp. 1710–1716 vol.2. [Online]. Available: <http://dx.doi.org/10.1109/ROBOT.2002.1014788>
- [11] Tsagarakis, N.G., Metta, G., Sandini, G., Vernon, D., Beira, R., Becchi, F., Righetti, L., Santos-Victor, J., Ijspeert, A.J., Carrozza, M.C., Caldwell, and D.G., "icub: the design and realization of an open humanoid platform for cognitive and neuroscience research," *Advanced Robotics*, vol. 21, no. 10, pp. 1151–1175, 2007. [Online]. Available: <http://dx.doi.org/10.1163/156855307781389419>
- [12] J. K. Salisbury, W. T. Townsend, D. M. DiPietro, and B. S. Eberman, "Compact cable transmission with cable differential," Patent, Feb. 1990, uS 4 903 536.
- [13] "Barrett Technology Inc. website," <http://www.barrett.com/robot/products-arm.htm>, Jun. 2009.
- [14] F. Aghili, M. Buehler, and J. Hollerbach, "A joint torque sensor for robots," in *In ASME International Mechanical Engineering Congress & Exposition*, 1997.
- [15] D. Vischer and O. Khatib, "Design and development of high-performance torque-controlled joints," in *Proc. IEEE Int. Conf on Robotics and Automation*, 1995, pp. 537–544.
- [16] G. Cheng, H. Sang-Ho, A. Ude, J. Morimoto, J. Hale, J. Hart, J. Nakanishi, D. Bentivegna, J. Hodgins, C. Atkeson, M. Mistry, S. Schaal, and M. Kawato, "Cb: Exploring neuroscience with a humanoid research platform," *Advanced robotics*, vol. 21, no. 10, pp. 1097–1114, 2007.
- [17] S. P. Timoshenko and J. Goodier, *Theory of Elasticity*. McGraw-Hill, 1970.

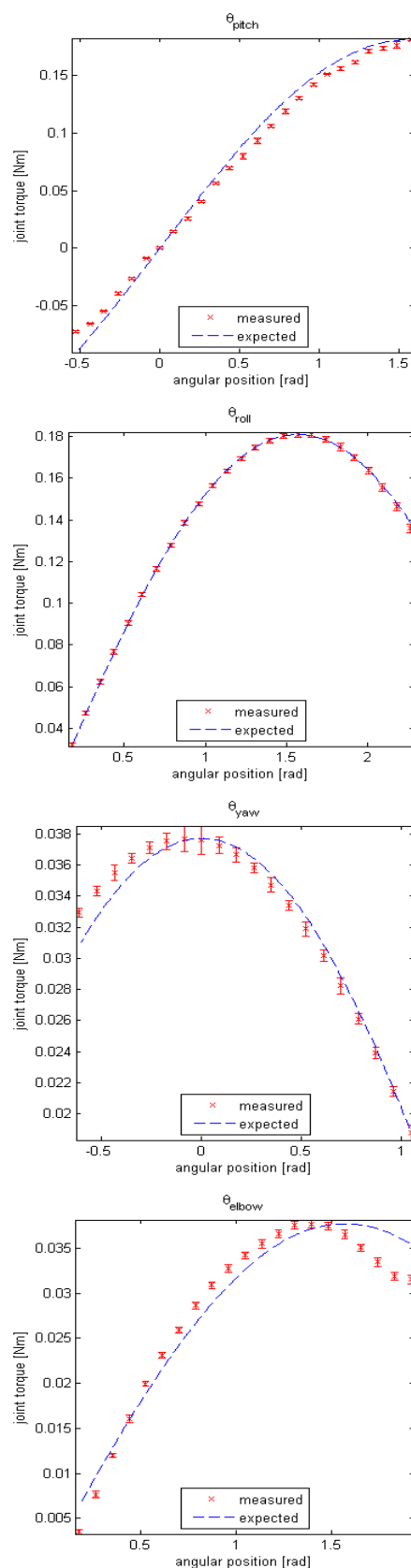


Fig. 8. Sensor validation. The joint torque measurements on the shoulder pitch, shoulder roll and elbow joints are shown in (a), (b), and (c) respectively.